Structure formation and the morphology diagram of possible structures in two-dimensional diffusional growth

E. Brener,* H. Müller-Krumbhaar, and D. Temkin†
Institut für Festkörperforschung, Forschungszentrum Jülich, D-52425 Jülich, Germany
(Received 20 March 1996)

The morphology diagram of possible structures in two-dimensional diffusional growth is given in the parameter space of undercooling Δ versus anisotropy of surface tension ϵ. The building block of the dendritic structure is a dendrite with parabolic tip, and the basic element of the seaweed structure is a doublon. The transition between these structures shows a jump in the growth velocity. We also describe the structures and velocities of fractal dendrites and doublons destroyed by noise. We introduce a renormalized capillary length and density of the solid phase and use scaling arguments to describe the fractal dendrites and doublons. The resulting scaling exponents for the growth velocity and the different length scales are expressed in terms of the fractal dimensions for surface and bulk of these fractal structures. All the considered structures are compact on length scales larger than the diffusion length and they show fractal behavior on intermediate length scales between the diffusion length and a small size cutoff which depends on the strength of noise. [S1063-651X(96)04209-2]

PACS number(s): 81.10.Aj

I. INTRODUCTION

The growth of a crystal from the melt or from a solution is a typical example for structure formation process [1]. This type of phase change usually requires the transport of at least one conserved quantity, the solute material or the latent heat of solidification, which is transported via diffusion. This is about the simplest pattern-forming process conceivable under essentially homogeneous nonequilibrium conditions. Mathematically this is known under the name *Stefan* [2] or *moving boundary* problem. Some of the basic questions one would like to answer in this context concern the kind of structures that can be formed by such an advancing interface and how the structures and the conditions under which they are formed can be characterized.

It has been known since about three decades ago [3] that a growing circular nucleus becomes unstable as its radius becomes bigger than a few times the critical radius. If the surface tension is anisotropic, for example due to crystalline anisotropy, it is generally believed that the nucleus finally deforms into a dendritic pattern like a snowflake [4]. The limit of vanishing anisotropy, however, is still somewhat less clear, although substantial progress was made during the past three years.

There has been a recent attempt to formulate a theory [5] for the fundamental morphologies of growth patterns under diffusion and the most relevant parameters controlling their appearance. This was based on scaling relations together with asymptotic matching requirements so that solutions expected in some limits of the parameters would be recovered. The morphology-diagram [5] uses *supercooling vs anisotropy* as the principal axes and discriminates between seaweed and dendrites as the basic patterns, where the dendritic patterns are characteristic for anisotropic growth conditions. A second classification concerns the patterns' internal structures, namely, fractal as opposed to compact patterns. A fractal pattern is one with a self-similar or self-affine internal structure with a scaling range of at least one order of magnitude in length scales. The fractal region in parameter-space is similar to the critical region in critical phenomena and accordingly a similar changeover to the nonfractal compact region may occur without any singularity. Some basic predictions of this theory [5] can be summarized as follows.

The dendritic pattern was predicted to compete at low anisotropies and large driving force with a compact seaweed growth mode which should still grow at a nonzero velocity even when the anisotropy has completely vanished. This was recently confirmed numerically in detail [6]. The compact seaweed growth-mode was conjectured to be an independent growth mode already several years ago under the name ''dense branching morphology'' [7].

At low supercoolings and at low anisotropies the dendritic structures furthermore were predicted to break up into fractal dendrites [5] in the presence of noise. The seaweed structures were predicted to evolve into fractal patterns under these conditions. Their fractal dimension was expected to be equal to the one obtained in atomistic simulations [8] of the Laplace-aggregation. This behavior was also confirmed [6] within the available numerical precision.

When this previous paper [5] was written, however, the existence of *doublons* as the basic building blocks for seaweed-structures in two dimensions was not known. The recent developments of parity-broken diffusional growth fingers in a channel [6,9–11] and free doublons [12,13] gave substantial new insight into the mechanism of seaweed growth both for compact and fractal morphology and also considering the possible competition with the dendritic growth mode. Furthermore, the description of growing fractal structures seems to require a renormalization of the sur-

*Permanent address: Institute for Solid State Physics, Chernogolovka, Russia.
†Permanent address: I.P. Bardin Institute of Ferrous Metals, Moscow, Russia.

face energy which has not been performed so far. We found it therefore necessary to address the question of the morphology diagram again in the light of these recent observations.

II. FORMULATION OF THE PROBLEM

We are interested in a nonequilibrium situation—growth of a stable phase from a metastable one. To be specific, we consider the two-dimensional growth of a pure substance from its undercooled melt, where the growth is controlled by the diffusion of the latent heat of freezing. It obeys the diffusion equation and appropriate boundary conditions at the moving interface

$$\frac{\partial U}{\partial t} = D\nabla^2 U, \tag{1}$$

$$v_n = D\vec{n}\cdot(\vec{\nabla}U_s|_{int} - \vec{\nabla}U_L|_{int}), \tag{2}$$

$$U|_{int} = \Delta - d(\Theta)K. \tag{3}$$

The indices L and S refer to the liquid and solid, respectively. The specific heat c_p and the thermal diffusion constant D are considered to be the same in both phases, L is the latent heat; $U=(T-T_\infty)c_p/L$ is the appropriately rescaled temperature field measured from the imposed temperature T_∞ of the undercooled melt far away from the interface; in terms of these parameters,

$$\Delta = (T_M - T_\infty)c_p/L \tag{4}$$

is the dimensionless undercooling of the melt and T_M is the melting temperature.

The physics underlying Eqs. (1)–(3) is quite simple. A solidifying front releases latent heat which diffuses away as expressed by Eq. (1); requiring heat conservation at the interface gives Eq. (2) ($\vec{n}$ is the normal to the interface). Equation (3) is local equilibrium condition at the interface which takes into account the Gibbs-Thomson correction; K is the two-dimensional curvature and $d(\Theta)$ is the so-called anisotropic capillary length with an assumed fourfold symmetry,

$$d(\Theta) = d_0(1-\epsilon\cos 4\Theta). \tag{5}$$

Here $d_0=\gamma T_M c_p/L^2$ is a capillary length proportional to the isotropic part of the surface energy γ; Θ is the angle between the normal $\vec{n}$ to the interface and some fixed crystallographic direction, at which $d(\Theta)$ is minimal; ϵ is the strength of the anisotropy.

In Eq. (3) we neglect the kinetic effects, that is, the dependence of the interface temperature on the growth velocity v_n which holds at the sufficiently small undercoolings and velocities.

Our main interest here is concerned with patterns which can grow at constant speed even at low undercoolings $\Delta<1$, because if they exist they will dominate the system's behavior. A two-phase structure then must exist behind the growth front filling the space uniformly on sufficiently large scales. The fraction η of solid inside this two-phase region should be equal to Δ due to global conservation,

$$\eta = \Delta. \tag{6}$$

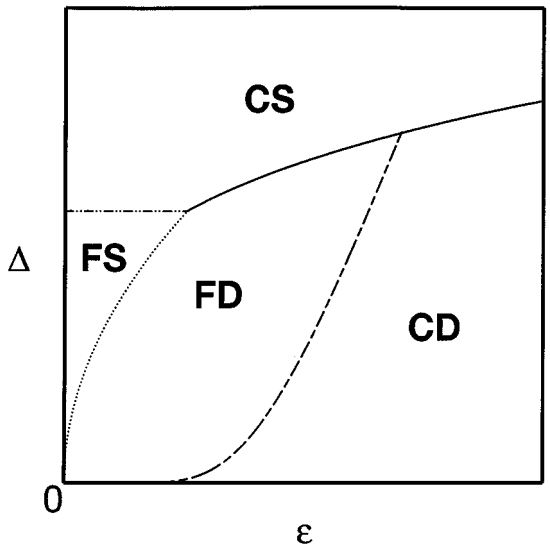

FIG. 1. Kinetic phase diagram.

One may define an envelope over the front of this complex two-phase structure, calling this suitably averaged envelope the *average front* in contrast to the local interface separating the solid from the liquid. This average front can be considered as the real growth front in the sense that a two-phase mixture, solid plus liquid, grows into a one-phase region originally consisting of liquid only. These two-phase structures are developed from initially smooth interfaces by the well-known Mullins-Sekerka instability.

Equations (1)–(5) contain two dimensional parameters, d_0 and D, and two dimensionless parameters, Δ and ϵ. It means that any characteristic length scale, ℓ, and growth velocity, v, of the possible structures can be presented in the form

$$\ell = d_0 f(\Delta,\epsilon), \quad v = \frac{D}{d_0}\varphi(\Delta,\epsilon). \tag{7}$$

Our aim in this paper is to predict, for given undercooling Δ and anisotropy ϵ, the type of the two-phase structure, and its characteristic length scales and velocity, that is, to calculate the functions f and φ in the relation (7). As it turns out these functions have scaling forms for small Δ and ϵ, thus showing power law dependences on Δ and ϵ.

Following the ideas of our previous paper [5] we try to construct the kinetic phase diagram in the plane (Δ,ϵ) (Fig. 1), which represents the regions of existence of different structures and the lines of transitions between the structures. As in, [5] we discriminate between *compact* structures (C) and *fractal* structures (F). A complementary classification deals with the existence of orientational order. A structure with pronounced orientational order will be called *dendritic* (D), and without apparent orientational order it will be called *seaweed* (S).

It turns out that noise which always exists in the system (for example the thermodynamic noise) appears to play a crucial role in the formation of fractal structures but is not so important for compact patterns.

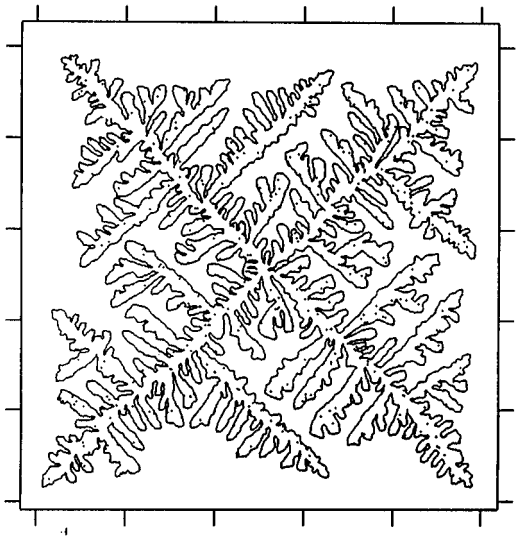

FIG. 2. Dendritic structure. For details, see Ref. [5].

III. COMPACT DENDRITES (CD)

Dendrites can grow at arbitrary small undercooling Δ, but usually a nonzero value of the anisotropy ϵ is required. The growth pattern evolving from a nucleus acquires a star-shaped envelope surrounding a well-defined backbone. The distances between the corners of the envelope increase with time. For small undercooling we can use the scaling relation for the motion of the corners as for free dendrites [14–17] with tip-radius ρ_t and velocity v. These two relations come from the Ivantsov formula [18]

$$P \equiv \frac{v\rho_t}{2D} \sim \Delta^2 \tag{8}$$

and from the selection condition for the stability parameter σ,

$$\frac{1}{\sqrt{\sigma}} \equiv \frac{\rho_t}{\sqrt{d_0 D/v}} \sim \epsilon^{-7/8}. \tag{9}$$

From Eqs. (8) and (9) follow the dependencies of ρ_t and v on the parameters Δ and ϵ:

$$\rho_t \sim d_0 \epsilon^{-7/4} \Delta^{-2}, \quad v \sim \frac{D}{d_0} \epsilon^{7/4} \Delta^4. \tag{10}$$

Equation (10) really describes a needle-crystal which without noise has no sidebranches. The corresponding star structure then cannot fill the space with constant density and the amount of material solidified in parabolic form increases with time only like $t^{3/2}$ rather than like t^2 for a truly compact object in two dimensions.

A small amount of noise, however, cures this problem. The tip of the dendrite is still stable against small noise but has a ''convective'' instability which produces sidebranches. Those branches continue to grow until they become independent primary branches a distance $\ell = D/v$ away from the corners of the star. The global shape then consists of an envelope of diamond type over the dendrite tips which appear a distance D/v apart from each other (Fig. 2). The velocity scales like Eq. (10). The relative space filling by primary dendrites and sidebranches of course must be equal to Δ. The two basic length scales in this pattern accordingly are the diffusion length D/v and the tip radius ρ_t of a typical dendrite.

For small undercooling Δ those two length scales are well separated, $\rho_t \ll D/v$. While the dendritic structure becomes compact only at length scales larger than D/v, it shows fractal behavior at the intermediate length scale ℓ, $\rho_t < \ell < D/v$, with fractal dimension $D_f = 1.5$ [19,20]. In this fractal object the sidebranches interact due to the competition in the common diffusion field. Some of the sidebranches die and some continue to grow in the direction prescribed by the anisotropy. This competition leads to coarsening of the structure in such a way that the distance between the surviving sidebranches is adjusted to be of the same order of magnitude as the length of the sidebranches and is proportional to the distance from the dendritic tip. At the same time, the thickness of the surviving sidebranches is proportional to the square root of the product of ρ_t and the distance from the tip. On length scales larger than D/v the dendritic structure appears to be compact with the mean density $\eta = \Delta$.

IV. COMPACT SEAWEED (CS)

CD structures formally exist at arbitrary small anisotropy ϵ but their velocity goes to zero with $\epsilon \to 0$. It was recently discovered that there is another structure, compact seaweed (CS), which is favorable for smaller ϵ and larger Δ. The velocity of the structure remains finite at $\epsilon = 0$.

The *compact-seaweed* morphology [5] was originally introduced on the basis of experimental observations under the name *dense branching* morphology [7]. At that time, however, its introduction as a morphological ''phase'' distinct from the well-known dendritic morphologies was rather speculative. Computer simulations also were inconclusive at that time.

The first indication for the existence of such a distinct phase came (to our knowledge) from arguments [5] based on a theoretical study of crystal growth in a channel [21]. This analysis of channel growth gave among other things the following results. A finger type pattern symmetrically in the center of the channel could grow at constant growth rate for dimensionless supercoolings $\Delta > 0.5$. The finger looks similar to the Saffmann-Taylor finger of viscous flow, but belongs to a different branch of the mathematical solution. The growth rate of the crystal increases with increasing driving force Δ, as to be expected. A specifically remarkable result of this theory [21] is that the driving force sets a length scale and thereby also a velocity: For a given driving force $0.5 < \Delta < 1$ there exists a characteristic channel width below which such a steadily growing finger is no longer possible.

However, it has been discovered recently that the spectrum of solutions for growth in a channel is much richer than had previously been supposed. Parity-broken solutions were found [9] and studied numerically in detail [6,10]. A similar solution exists also in an infinite space which was called ''doublon'' for obvious reasons [6]. It consists of two fingers with a liquid channel along the axis of the symmetry between them. It has a parabolic envelope with radius ρ_t and the liquid channel of the thickness h. The Peclet number

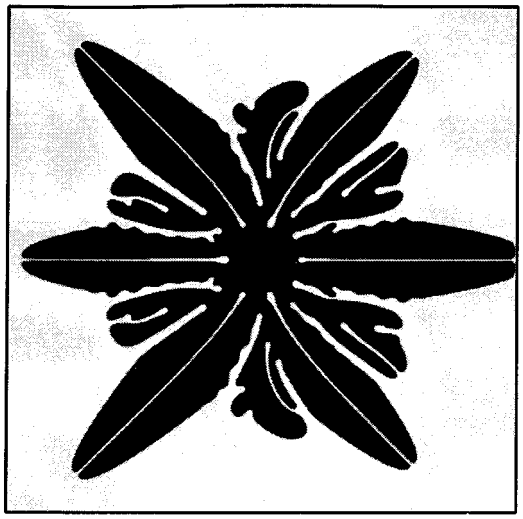

FIG. 3. Seaweed structure [T. Abel and H. Müller-Krumbhaar (unpublished)].

$P=v\rho_t/2D$ depends on Δ according to the Ivantsov relation (8). The analytical solution of the selection problem for doublons [13] shows that this solution for isotropic systems ($\epsilon=0$) exists even at arbitrary small undercooling Δ and obeys the following selection conditions:

$$h\sim\rho_t, \quad \frac{1}{\sqrt{\sigma}}\equiv\frac{\rho_t}{\sqrt{d_0D/v}}\sim P^{-5/4}. \tag{11}$$

Equations (8) and (11) give

$$\rho_t\sim h\sim d_0\Delta^{-7}, \quad v\sim\frac{D}{d_0}\Delta^9. \tag{12}$$

If one includes finite anisotropy ϵ, doublon solutions exist only above the solid line on Fig. 1, for which

$$\Delta\sim\epsilon^{1/4}. \tag{13}$$

For ϵ smaller than given by Eq. (13) the doublons obey the same scaling law as given by Eq. (12) [13].

It should be noted that doublons in the range of their existence (13) grow faster than dendrites at the same parameters Δ and ϵ. This statement is confirmed by numerical calculations [6].

The numerical calculations also show that the double-fingering structure is stable against a competition between the two fingers which belong to the doublon. It means that the axis of symmetry and the direction of growth are stable. Of course these directions are arbitrary in isotropic systems. It is not completely clear at the moment whether the stability of the free doublon pair follows precisely the scaling law Eq. (13). In any case this line represents a lower bound on Δ for a given ϵ.

We suppose that the doublons seem to represent a key point in the growth of compact-seaweed morphology (Fig. 3). The formation of a full CS structure evolving from a growing nucleus is possible only due to noise, which triggers sidebranches, as it is in the CD structure. The resulting two-phase structure has an almost isotropic circular envelope which moves with approximately the same velocity [Eq. (12)] as a free doublon. The structure is fractal with $D_f=1.5$ in the intermediate length scale between ρ_t and D/v, and it becomes compact with the mean density $\eta=\Delta$ at the length scale larger than D/v. The region above the solid line, $\Delta\sim\epsilon^{1/4}$ (Fig. 1), corresponds to CS structure where doublons exist and grow faster than dendrites. This line represents the discontinuous transitions between CD and CS structures with a jump of velocities.

V. FRACTAL STRUCTURES

For the compact structures described above noise is important only as the trigger of sidebranches. It has been supposed that the tips (of dendrites or doublons) remain undestroyed. However, the strength of noise may be large enough not only to trigger the sidebranches but also to destroy the tips. In order to estimate the parameters for which it happens let us look at the theory of sidebranch-formation more carefully. According to the result of Langer [22] the root-mean-square amplitude $\langle\zeta^2\rangle^{1/2}$ of the sidebranches on the underlying parabolic interface generated by thermal fluctuations depends on the distance from the tip z as

$$\frac{\langle\zeta^2\rangle^{1/2}}{\rho_t}\sim\Gamma\exp\left[\frac{2^{7/4}}{3\sqrt{3\sigma}}\left(\frac{z}{\rho_t}\right)^{1/4}\right]. \tag{14}$$

Here the stability parameter σ is given by Eqs. (9) and (11) for dendrites and doublons, respectively; Γ is the relative noise strength ($\Gamma\ll1$)

$$\Gamma=(T/T_o)\left(\frac{2Dd_0^3}{v\rho_t^4}\right)^{1/2}, \quad T_o=\left(\frac{L^2d_0^3}{k_Bc_p}\right)^{1/2}, \tag{15}$$

where k_B is the Boltzmann constant. The tip becomes destroyed if the amplitude of the sidebranches is of the order of ρ_t at the distance $z\sim\rho_t$ down the shaft. Thus we obtain from Eq. (14) the following condition:

$$\frac{1}{\sqrt{\sigma^*}}\sim|\ln\Gamma|. \tag{16}$$

The tips of structures will be destroyed if the stability parameter σ becomes smaller than the critical value σ^* given by Eq. (16). Using the value $\sigma\sim\epsilon^{7/4}$ [Eq. (9)], one obtains from Eq. (16) a line of smooth transition from CD to FD structures on Fig. 1:

$$\epsilon^*\sim|\ln\Gamma|^{-8/7}. \tag{17}$$

The analogous line which separates CS and FS structures in Fig. 1 can be obtained using Eqs. (8), (11), and (16):

$$\Delta^*\sim|\ln\Gamma|^{-2/5}. \tag{18}$$

Equation (16) has the following physical meaning. Let us rewrite this relation, using the definition of $\sigma=d_0D/(v\rho_t^2)$ [Eq. (9)], which gives the following condition for a stable tip radius:

$$\rho_t\leqslant\rho_{MS}|\ln\Gamma|, \tag{19}$$

where $\rho_{MS}\sim\sqrt{d_0D/v}$ is the Mullins-Sekerka length describing the instability of a planar interface. One can think of the right-hand side of (19) as the characteristic length scale, a_Γ, of the instability set by noise

$$a_\Gamma=\rho_{MS}|\ln\Gamma|\sim\sqrt{d_0D/v}|\ln\Gamma|. \tag{20}$$

The tip is stable if $\rho_t<a_\Gamma$ and it becomes destroyed if $\rho_t>a_\Gamma$. The same small-size cutoff a_Γ depending on noise Γ was introduced in our previous paper [5] based on the consideration of the self-similar development of perturbations induced by the Mullins-Sekerka instability. At that time, however, the existence of doublons was not known.

A new approach, therefore, is required for the description of the fractal patterns with the destroyed tips. Such destroyed fractal structures have been already investigated in the framework of Saffmann-Taylor viscous fingering and diffusion-limited aggregation [19]. The important result of these investigations is that there exists an effective envelope obtained by averaging over the structures, which has precisely the same shape as an ideal stable solution—the shape of the Saffman-Taylor finger in isotropic systems and parabolic shape in anisotropic systems. The density inside this effective envelope is $\widetilde{\eta}<1$. The envelope has a characteristic tip radius $\widetilde{\rho}_t$. Because the underlying structure is fractal with fractal dimension $D_f\approx1.71$ in the intermediate length scale between small-length cutoff a_Γ and $\widetilde{\rho}_t$, the density $\widetilde{\eta}$ inside the envelope can be obtained from the definition of the fractal dimension (apart from a constant prefactor)

$$\widetilde{\rho}_t^{D_f}\sim\int_{a_\Gamma}^{\widetilde{\rho}_t}drr\widetilde{\eta}(r),$$

which gives more explicitly

$$\widetilde{\eta}(\widetilde{\rho}_t)\sim\left(\frac{a_\Gamma}{\widetilde{\rho}_t}\right)^{2-D_f}. \tag{21}$$

Following these results, we will now try to define an averaged or coarse-grained structure over such a noisy fractal pattern and to formulate an equation of motion for this coarse-grained structure using scaling arguments. More explicitly we try to estimate the characteristic length scale of the structure and its growth velocity by considering the steady-state motion of an effective parabolic envelope which replaces the destroyed dendrite or doublon. The density of the solid phase inside the envelope with tip radius $\widetilde{\rho}_t$ is given by Eq. (21), where the small size cutoff a_Γ is defined by Eq. (20),

$$\widetilde{\eta}(\widetilde{\rho}_t)\sim\left(\frac{\sqrt{d_0D/v}|\ln\Gamma|}{\widetilde{\rho}_t}\right)^{2-D_f}. \tag{22}$$

The temperature inside the envelope is supposed to be close to the melting temperature. Because the density $\widetilde{\eta}$ inside the envelope is smaller than 1, we have to replace the latent heat L by $\widetilde{\eta}L$. It changes Δ in Eq. (4) to $(\Delta/\widetilde{\eta})$ and modifies the Ivantsov relation to

$$P\equiv\frac{v\widetilde{\rho}_t}{2D}\sim\left(\frac{\Delta}{\widetilde{\eta}}\right)^2. \tag{23}$$

The crucial point of the analysis is a modification of the selection conditions (9) and (11). The experimental and numerical results [19] (the existence of a selected envelope) support the idea that those selection conditions do exist. Unfortunately, we do not know any results which allow us to write down these modifications explicitly. But using scaling arguments, we can write the selection conditions in the following scaling form with scaling exponent β which for the moment is undetermined but will be specified later in the following section. For dendrites we can write

$$\frac{1}{\sqrt{\sigma}}\equiv\frac{\widetilde{\rho}_t}{\sqrt{d_0D/v}}\sim\epsilon^{-7/8}\widetilde{\eta}^{-\beta} \tag{24}$$

and for doublons

$$\frac{1}{\sqrt{\sigma}}\equiv\frac{\widetilde{\rho}_t}{\sqrt{d_0D/v}}\sim P^{-5/4}\widetilde{\eta}^{-\beta}. \tag{25}$$

These relations (24) and (25) transform into Eq. (9) and Eq. (11), respectively, for $\widetilde{\eta}\sim1$.

The selection relations (24) and (25) may be interpreted as the conditions of selection due to an effective surface tension. We have chosen the same β in both Eqs. (24) and (25) because in some sense the factor $\widetilde{\eta}^{-\beta}$ can be seen as a renormalization factor for the capillary length $d_0\to d_0/\widetilde{\eta}^{2\beta}$. To make an estimate of possible values of β it is natural to assume that a coarse-grained surface energy should decrease with decreasing $\widetilde{\eta}$, giving $\beta<1/2$ as a reasonable restriction. Furthermore, under the speculation that not only the latent heat L transforms to $\widetilde{\eta}L$ but also the surface energy γ for the solid-liquid interface transforms similarly into $\widetilde{\eta}\gamma$ for the coarse-grained envelope, we find that d_0 remains unchanged. For this simplest model one obtains $\beta=0$ which has been used in our previous publication [5]. We will not follow this reasoning but will see later that with much more conclusive arguments β can be expressed in terms of bulk and surface fractal dimensions.

The solution of Eqs. (22)–(25) gives the following for general fixed β.

For *fractal dendrites*,

$$\widetilde{\rho}_t\sim\frac{d_0}{\Delta^2}\frac{|\ln\Gamma|^2}{(|\ln\Gamma|\epsilon^{7/8})^{2\gamma(D_f-1)}}, \tag{26}$$

$$v\sim\frac{D}{d_0}\frac{\Delta^4}{|\ln\Gamma|^2}(|\ln\Gamma|\epsilon^{7/8})^{2\gamma(2D_f-3)}, \tag{27}$$

$$\widetilde{\eta}(\widetilde{\rho}_t)\sim(|\ln\Gamma|\epsilon^{7/8})^{\gamma(2-D_f)}, \tag{28}$$

for

$$\Delta<(|\ln\Gamma|\epsilon^{7/8})^{\gamma(2-D_f)}<1, \tag{29}$$

where

$$\gamma=1/[1-\beta(2-D_f)]. \tag{30}$$

For *fractal doublons*,

$$\widetilde{\rho}_t \sim \frac{d_0}{\Delta^2}\frac{|\ln\Gamma|^2}{(|\ln\Gamma|\Delta^{5/2})^{2\gamma'(D_f-1)}}, \tag{31}$$

$$v \sim \frac{D}{d_0}\frac{\Delta^4}{|\ln\Gamma|^2}(|\ln\Gamma|\Delta^{5/2})^{2\gamma'(2D_f-3)}, \tag{32}$$

$$\widetilde{\eta}(\widetilde{\rho}_t) \sim (|\ln\Gamma|\Delta^{5/2})^{\gamma'(2-D_f)}, \tag{33}$$

for

$$\Delta < (|\ln\Gamma|\Delta^{5/2})^{\gamma'(2-D_f)} < 1 \tag{34}$$

and

$$\Delta > \epsilon^{1/4}(|\ln\Gamma|\Delta^{5/2})^{\gamma'(2-D_f)}, \tag{35}$$

where

$$\gamma' = 1/[1+(5/2-\beta)(2-D_f)]. \tag{36}$$

Equation (35) which has no analog among Eqs. (26)–(30) for fractal dendrites is similar to Eq. (13) for compact doublons and defines a region of parameters where the fractal doublons do exist; on the boundary of the region (dotted line in Fig. 1) the doublon solutions disappear.

Fractal dendrites and fractal doublons exist in the range of parameters given by inequalities (29) and (34), respectively, which correspond to $\Delta < \widetilde{\eta}(\widetilde{\rho}_t) < 1$. The upper boundaries $[\widetilde{\eta}(\widetilde{\rho}_t) \sim 1]$, $|\ln\Gamma|\epsilon^{7/8} \sim 1$, and $|\ln\Gamma|\Delta^{5/2} \sim 1$ correspond to the transition to compact structures (dashed line and dash-dotted line on the diagram of the Fig. 1). The lower boundaries in conditions (29) and (34) correspond to $\widetilde{\eta} \sim \Delta$ (and at the same time correspond to $\widetilde{\rho}_t \sim D/v$). The described structures are fractal with $D_f \approx 1.7$ on the length scale between a_Γ and $\widetilde{\rho}_t$, and fractal with $D_f = 1.5$ in the range between $\widetilde{\rho}_t$ and D/v; the structures become compact with $\eta = \Delta$ on the length scale larger than D/v.

Equations (26)–(36) describe fractal dendrites and doublons as long as $a_\Gamma < \widetilde{\rho}_t < D/v$. If $\widetilde{\rho}_t$ becomes formally larger than D/v, the patterns are fractal with $D_f \approx 1.7$ in the range between a_Γ and D/v, and compact on the scale larger than D/v with density $\eta = \Delta$. The growth velocity of this last structure can easily be obtained from Eq. (22) by replacing $\widetilde{\rho}_t$ by D/v and by setting $\widetilde{\eta}(\widetilde{\rho}_t) \sim \Delta$:

$$v \sim \frac{D}{d_0}\frac{\Delta^{2/(2-D_f)}}{|\ln\Gamma|^2}. \tag{37}$$

This velocity matches to the velocity of the fractal dendrite (27) at the line

$$\Delta \sim (|\ln\Gamma|\epsilon^{7/8})^{\gamma(2-D_f)}, \tag{38}$$

which corresponds to the lower boundary of the condition (29). The lower boundary in relation (34) gives a transition from fractal doublons to the structure described by Eq. (37). The last structure which moves with velocity given by Eq. (37) has been already described in our previous papers [5] as representing the fractal seaweed morphology. The doublons as an independent pattern were not yet discovered at that time. Now we can see for reasonable values of $\beta < 1/2$ that the structure described by Eq. (37) disappears from the morphology diagram on Fig. 1. The point is that the formal line given by Eq. (38), which describes the transition from fractal dendrites to the structure growing in accord to Eq. (37), is located in the region of fractal doublons, where the doublons grow faster compared to the two other structures. Thus the dotted line on Fig. 1 given by condition (35),

$$\Delta \sim |\ln\Gamma|^{\psi_\Gamma}\epsilon^{\psi_\epsilon},$$

$$\psi_\Gamma = \frac{2-D_f}{1-\beta(2-D_f)},$$

$$\psi_\epsilon = \frac{1+(5/2-\beta)(2-D_f)}{4[1-\beta(2-D_f)]}, \tag{39}$$

describes the discontinuous transition from fractal dendrites (FD) to fractal doublons (FS) with a jump of growth velocity.

All the characteristics of fractal structures depend on the noise strength Γ. We can estimate Γ in the fractal region using Eq. (15) and replacing ρ_t by the noise induced length scale a_Γ from Eq. (20). It gives

$$\Gamma|\ln\Gamma|^2 \sim \left(\frac{T}{T_o}\right)\left(\frac{v d_0}{D}\right)^{1/2}. \tag{40}$$

The noise strength $\Gamma \ll 1$ because the capillary length d_0 is much smaller than the diffusion length D/v.

VI. SCALING OF COARSE GRAINED CAPILLARY LENGTH

We now will try to relate the scaling exponent β to the fractal exponents describing the fractal dimension D_s of the surface and the fractal dimension D_f of the bulk of the respective noisy structures which we have defined above as fractal doublons and fractal dendrites.

The idea is that the fractal dendrite as a noisy object should be describable in a similar form as the original compact dendrite because the basic Ivantsov-relation Eq. (23) represents a global conservation law. The ingredients of that description such as capillary length or density inside that envelope, however, then should be in some way renormalized.

We assume now that a noisy dendrite can be described by an effective envelope with a constant mean density $\widetilde{\eta}$ of solid inside. Furthermore, we assume that also the Gibbs-Thomson relation Eq. (3) has to be modified by introducing an effective capillary length $\widetilde{d}_0$ and a macroscopic curvature $\widetilde{K}$ of the smoothed envelope. The Gibbs-Thomson relation (3) then becomes

$$U|_{int} = \frac{\Delta}{\widetilde{\eta}} - \frac{\widetilde{d}_0}{\widetilde{\eta}}[1-\epsilon\cos(4\Theta)]\widetilde{K}, \tag{41}$$

where $\widetilde{\eta}$ represents the mean density inside that approximately parabolic envelope over a single dendrite. Note that

the density η averaged over the whole solidified structure on scales larger than the diffusion length is still given by Eq. (6).

The first term on the right-hand side of Eq. (41) represents the modification of the conservation-law due to the deviation from compactness, $\tilde{\eta}<1$. The second term is actually a definition of effective capillarity $\tilde{d}_0$ through the geometrical definition of local curvature $\tilde{K}$ of the parabolic envelope. This coarse-grained envelope should then evolve in analogy to Eq. (9) (for the dendritic case) but now with the coarse-grained variables as

$$\frac{1}{\sqrt{\sigma}} \equiv \frac{\tilde{\rho}_t}{\sqrt{\tilde{d}_0 D/(\tilde{\eta} v)}} \sim \epsilon^{-7/8}. \tag{42}$$

Note that not only the rescaled capillary length but also the density $\tilde{\eta}$ appear here because we have chosen $\tilde{\eta}$ as a common denominator in Eq. (41). Combining Eq. (42) with Eq. (24) one obtains formally the relation

$$\tilde{d}_0 \sim d_0 \tilde{\eta}^{1-2\beta}, \tag{43}$$

which holds both for doublons and dendrites.

In order to relate such a coarse-grained capillary-length to the fractal properties of the growing structure we first must introduce a coarse-graining length $\tilde{\ell}$ as some arc-length of the resulting effective envelope. The coarse-grained contribution of curvature to the Gibbs-Thomson relation (41) on that envelope can be defined as an average over the local curvature contribution as (for simplicity shown for the isotropic case)

$$\tilde{d}_0 \tilde{K} = d_0 \frac{\int_{\tilde{\ell}} dl K}{\int_{\tilde{\ell}} dl}. \tag{44}$$

The integrals are performed within a neighborhood of diameter $\tilde{\ell}$ at some point on the envelope, the path of integration going along the real folding interface with K being the rapidly varying curvature of this real interface.

The result of this integration comes directly from the geometric definition of a curvature $K = d\Theta/dl$ as follows:

$$\frac{\int_{\tilde{\ell}} d\ell K}{\int_{\tilde{\ell}} d\ell} = \frac{\delta\Theta(\tilde{\ell})}{\ell(\tilde{\ell})}. \tag{45}$$

Note that $\ell(\tilde{\ell})$ here is the arc-length along the real interface around some fixed point on the envelope as a function of the coarse-graining length $\tilde{\ell}$. Furthermore, $\delta\Theta$ is the change of orientation of the envelope over a small tangential distance $\tilde{\ell}$. From this one immediately obtains the definition of the curvature $\tilde{K}$ by identifying

$$\tilde{K} \equiv \frac{\delta\Theta(\tilde{\ell})}{\tilde{\ell}} = \frac{\ell \delta\Theta(\tilde{\ell})}{\tilde{\ell}\, \ell(\tilde{\ell})}. \tag{46}$$

A combination of this result and Eq. (44) gives the desired result of the renormalized capillary length $\tilde{d}_0$:

$$\tilde{d}_0 = d_0(\tilde{\ell}/\ell). \tag{47}$$

This result looks trivial at first glance but in fact when the surface becomes fractal the length ℓ becomes much bigger than the coarse-graining length $\tilde{\ell}$ and can be expressed by a power-law dependence:

$$\ell \sim \tilde{\ell} \left(\frac{\tilde{\ell}}{a_\Gamma} \right)^{D_s - 1}, \tag{48}$$

where D_s is the fractal dimension of the surface and more specifically in two dimensions the fractal dimension of the perimeter of the fractal structure. A relation $1 \leqslant D_s \leqslant D_f \leqslant 2$ here should hold between the various dimensions. The short-length cutoff a_Γ has been introduced before.

The coarse-graining length $\tilde{\ell}$ now can be defined as follows. It is obvious that this length is confined between the limits

$$a_\Gamma < \tilde{\ell} < \tilde{\rho}_t, \tag{49}$$

because it must be bigger than the short-length cutoff and should not be bigger than the smallest length scale appearing along the coarse-grained envelope. A further restriction can be obtained from an interesting observation made in the related problem of Laplacian growth [19]. There it was found that the scaling of the noisy finger in the channel could be mapped onto the theory of smooth fingers only if this coarse graining length is taken to scale with the upper bound

$$\tilde{\ell} \sim \tilde{\rho}_t. \tag{50}$$

Furthermore, the (constant) density inside the coarse-grained envelope had to be taken equal to the maximal density observed in the averaged density-profile. Then the scaling of this density with the tip-radius of the envelope became consistent with the fractal scaling relation Eq. (21). We therefore adapt the same relations which are expected to be valid as long as the length-scales under consideration are small compared to the diffusion length.

Combining Eqs. (21) with Eqs. (47), (48), and (50) we arrive at the desired relation for the coarse-grained capillary length

$$\tilde{d}_0 \sim d_0 \tilde{\eta}^{(D_s - 1)/(2 - D_f)}. \tag{51}$$

Comparing this result with Eq. (43) we obtain immediately the final formula for the exponent β depending on the fractal dimensions D_s and D_f for surface and bulk:

$$\beta = \frac{1}{2} \left(1 - \frac{D_s - 1}{2 - D_f} \right). \tag{52}$$

Inserting this into the set of results Eq. (26) through Eq. (36) makes all the scaling exponents depending on the two fractal dimensions D_s and D_f only. As an example for numerical values [6] we may use $D_f \approx 1.71$ and $D_s \approx 1.67$. This results in a value of $\beta \approx -0.66$, and the growth rate of a fractal doublon Eq. (32) then should depend on the supercooling Δ as

$$v \sim \frac{D}{d_0} \Delta^{\psi}, \quad \psi \approx 5.1. \tag{53}$$

Apparently this growth rate is faster than our earlier result [5] for fractal seaweed Eq. (37) because the exponent ψ here is smaller than the previous value of $2/(2-D_f)\approx 6.9$ in Eq. (37). This means that fractal doublons should be the winning pattern at small driving forces and small anisotropies.

VII. CONCLUSION

We have discussed the structure formation in diffusion-controlled growth. The given description refers to solidification of a pure undercooled melt but it also can be applied to growth of a pure solid from solution or isothermal solidification of a binary melt. More generally one may speak of systems with a conserved quantity growing by diffusion. The main control parameters of the process are dimensional undercooling Δ and the strength of the surface tension anisotropy ϵ. It turns out that the noise is also very important for the structure formation and we characterize it by the dimensionless quantity Γ.

The resulting morphology diagram (Fig. 1) with axes Δ vs ϵ classifies different kinds of structures and transitions between them.

The dendritic structure has pronounced orientational order and it is favorable for small Δ and relatively large ϵ. The seaweed structure does not require anisotropy and is favored for larger Δ and smaller ϵ. The transition between these two structures takes place around the solid line on Fig. 1 [Eq. (13)] which is continued by the dotted line [Eq. (39)] into the fractal region. This transition is discontinuous with a jump of velocities since the doublons move faster than the dendrites as soon as they exist. The main element of the dendritic structure is a dendrite with a parabolic tip (Fig. 2), and the main element of the seaweed structure is a doublon (Fig. 3). For compact dendritic and compact seaweed structures the tips of dendrites and doublons are stable against the noise, which is relatively small in these regions. The noise triggers sidebranches which fill the space and make the structures compact so that the mean density of solid phase is $\eta=\Delta$ on the length scale larger than D/v. In the intermediate region of lengths between tip radius ρ_t and diffusion length D/v the structure can be described as a fractal but with a trivial fractal dimension $D_f=3/2$ which comes from the parabolic shape of the dendrite.

The region of fractal dendritic and fractal seaweed structures near the origin of the morphology diagram is characterized by noise being sufficiently large to destroy even the tips of dendrites and doublons. It means that the noise induced length scale a_Γ [Eq. (20)] is smaller than $\tilde{\rho}_t$. In the range between a_Γ and $\tilde{\rho}_t$ the structures are fractal with a nontrivial fractal dimension D_f ($D_f\approx 1.71$). This is the reason why we called these structures ''fractal.'' Furthermore, these patterns are also fractal in the range between $\tilde{\rho}_t$ and D/v but again with the trivial fractal dimension $D_f=3/2$. Finally they become compact on length scales larger than the diffusion length D/v just as compact dendritic and compact seaweed structures. Note that if one would perform a measurement of the fractal dimension on length scales around the crossover length $\tilde{\rho}_t$ one would observe an interpolation between our two different values of D_f, the precise result depending on the interval chosen for the measurement. Since both the dendritic and the seaweed patterns maintain their basic identities inside the noisy region, the transitions from the compact to the fractal regions represent rather smooth changes in length scales.

We have described the structures and growth velocities of the destroyed fractal dendrites and doublons by introducing renormalized quantities for capillary length and density. We have quantitatively introduced an effective parabolic envelope following the results of [19]. The most nontrivial part of our analysis is a modification of the selection conditions [Eqs. (24) and (25)]. At this point we have used scaling arguments which leave us only with one undetermined scaling exponent β. This exponent subsequently is determined by the fractal dimensions D_s for the surface and D_f for the bulk of the growing pattern.

The scaling arguments given here for two-dimensional growth patterns formally can be extended in a straightforward fashion to three dimensions. For dendritic structures this seems to be perfectly permissible since the basic growth laws are rather similar in two and three dimensions [23,24]. For the seaweed patterns much less is known since our preliminary results there are still rather speculative. We hope to report on this in the near future.

ACKNOWLEDGMENTS

We appreciate the support of a grant from the Volkswagen-Stiftung. We also thank T. Ihle and T. Abel for many useful discussions.

[1] J.S. Langer, Rev. Mod. Phys. **52**, 1 (1980).
[2] L.I. Rubinstein, *The Stefan Problem*, Am. Math. Soc. Transl. Vol. 27 (American Mathematical Society, Providence, 1971).
[3] W. Mullins and R. Sekerka, J. Appl. Phys. **34**, 323 (1963).
[4] H. Müller-Krumbhaar and W. Kurz, in *Phase Transformation in Materials*, edited by P. Haasen (VCH-Verlag, Weinheim, 1991).
[5] E. Brener, H. Müller-Krumbhaar, and D. Temkin, Europhys. Lett. **17**, 535 (1992); E. Brener, H. Müller-Krumbhaar, and D. Temkin, Int. J. Mod. Phys. **C3**, 825 (1992).
[6] T. Ihle and H. Müller-Krumbhaar, Phys. Rev. Lett. **70**, 3083 (1993); Phys. Rev. E **49**, 2972 (1994).
[7] E. Ben-Jacob, G. Deutscher, P. Garik, N. Goldenfeld, and Y. Lereah, Phys. Rev. Lett. **57**, 1903 (1986).
[8] T.A. Witten and L.M. Sander, Phys. Rev. Lett. **47**, 1400 (1981); Phys. Rev. B **27**, 5686 (1983).
[9] E. Brener, H. Müller-Krumbhaar, Y. Saito, and D. Temkin, Phys. Rev. E **47**, 1151 (1993).
[10] R. Kupfermann, D. Kessler, and E. Ben-Jacob, Physica A **213**, 451 (1995).
[11] M. Ben Amar and E. Brener (unpublished).
[12] E. Brener, Y. Saito, H. Müller-Krumbhaar, and D. Temkin, Pis'ma Zh. Éksp. Teor. Fiz. **61**, 285 (1995) [JETP Lett. **61**, 285 (1995)].

[13] M. Ben Amar and E. Brener, Phys. Rev. Lett. **75**, 561 (1995).
[14] J. S. Langer, in *Chance and Matter*, edited by J. Souletie, J. Vannimenus, and R. Stora (Elsevier, Amsterdam, 1987).
[15] D.A. Kessler, J. Koplik, and H. Levine, Adv. Phys. **37**, 255 (1988).
[16] E.A. Brener and V.I. Mel'nikov, Adv. Phys. **40**, 53 (1991).
[17] Y. Pomeau and M. Ben Amar, in *Solids Far From Equilibrium*, edited by C. Goldréche (Cambridge University Press, Cambridge, 1992).
[18] G.P. Ivantsov, Dokl. Acad. Nauk. SSSR **58**, 567 (1947).
[19] A. Arneodo, Y. Couder, G. Grasseau, V. Hakim, and M. Rabaud, Phys. Rev. Lett. **63**, 984 (1989); Y. Couder, F. Argoul, A. Arneodo, J. Maurer, and M. Rabaud, Phys. Rev. A **42**, 3499 (1990); A. Arneodo, F. Argoul, Y. Couder, and M. Rabaud, Phys. Rev. Lett. **66**, 2332 (1991).
[20] E. Brener and D. Temkin, Phys. Rev. E **51**, 351 (1995).
[21] E. Brener, M. Geilikman, and D. Temkin, Zh. Éksp. Teor. Fiz. **94**, 241 (1988) [Sov. Phys. JETP **67**, 1002 (1988)].
[22] J.S. Langer, Phys. Rev. A **36**, 3350 (1987).
[23] M. Ben Amar and E. Brener, Phys. Rev. Lett. **71**, 589 (1993).
[24] E. Brener, Phys. Rev. Lett. **71**, 3653 (1993).